

Supplementary Information

Carbene-like Reactivity of Methoxy Groups in a Single Crystal SAPO-34 MTO Catalyst

Ivalina B. Minova,^a Michael Bühl,^a Santhosh K. Matam,^{b,c} C.
Richard A. Catlow,^{b,c,d} Mark D. Frogley,^e Gianfelice Cinque,^e Paul
A. Wright,^a Russell F. Howe^f

- a. EastCHEM School of Chemistry, University of St Andrews, St Andrews KY16 9ST
- b. UK Catalysis Hub, Research Complex at Harwell, Rutherford Appleton Laboratory, Oxford, OX11 0FA
- c. Cardiff Catalysis Institute, School of Chemistry, Cardiff University, Cardiff CF10 3AT
- d. Department of Chemistry, University College London, London WC1E 6BT
- e. MIRIAM beamline B22, Diamond Light Source, Harwell Science and Innovation Campus, Didcot, OX11 0DE
- f. Chemistry Department, University of Aberdeen, AB24 3UE; Email: r.howe@abdn.ac.uk

Table of Contents

1.	Synthesis and Characterisation of SAPO-34 and ZSM-5 Single Crystals for <i>Operando</i> IR Microspectroscopy.....	2
2.	Catalyst Evaluation	5
3.	Supplementary Infrared and Mass Spectra	6
4.	DFT Calculations.....	13
5.	References.....	16

1. Synthesis and Characterisation of Crystals

SAPO-34 crystals were prepared in a modified Kornatowski literature procedure¹ with reduced Si and excess P in the synthesis gel: H₃PO₄, 85% (6.12 g, 53 mmol), Al(OH)₃ (4.80 g, 50 mmol), morpholine (4.56 g, 52 mmol) were added to deionised water (35.18 g, 2.00 mol) and then fumed silica was slowly added (0.602 g, 10 mmol). The gel composition (1.0 Al(OH)₃: 1.06 H₃PO₄ : 0.2 SiO₂ : 40 H₂O : 1.05 morpholine) was stirred at 313 K for 16 h before being sealed in a Teflon lined autoclave (125 mL, Parr) and heated at 463 K for 5 d, without tumbling. The solid was recovered by vacuum filtration, washed with deionised water and dried overnight at 373 K. Prior to spectroscopic measurements, the crystals were freshly calcined at 823 K (2 K min⁻¹) in air for 14 h to give the proton form.

ZSM-5 crystals were prepared as described previously.²

Chemical analysis of the prepared SAPO-34 samples was performed using X-ray fluorescence spectroscopy (Panalytical Axios 4 kW rhodium tube X-ray generator). Samples were also characterised by thermogravimetric analysis, X-ray powder diffraction (with Cu-K α radiation), scanning electron microscopy (Hitachi S-4800). Solid-state MAS NMR spectra were acquired on a Bruker Advance III 400 MHz spectrometer equipped with a 9.4 T widebore superconducting magnet. Prior to obtaining quantitative ²⁷Al MAS NMR, the sample was left to hydrate overnight in a water-containing desiccator. The Brønsted acid sites were titrated with ammonia and quantified on a Micrometrics AutoChem II Chemisorption Analyzer. Nitrogen adsorption was carried out on a Micrometrics 3Flex which was equipped with 0.1, 10, and 1000 torr transducers on each port. Samples underwent a 2 stage degas procedure: first ex-situ at 673 K for 480 min, then in-situ under high vacuum at 623 K (8 K min⁻¹) for 4 h.

Figure S1 shows thermogravimetric analysis of as prepared SAPO-34 heated in air at 10 K min⁻¹. The 17 % weight loss above 600 K corresponds to decomposition of 1.7 morpholine molecules per *cha* cage.

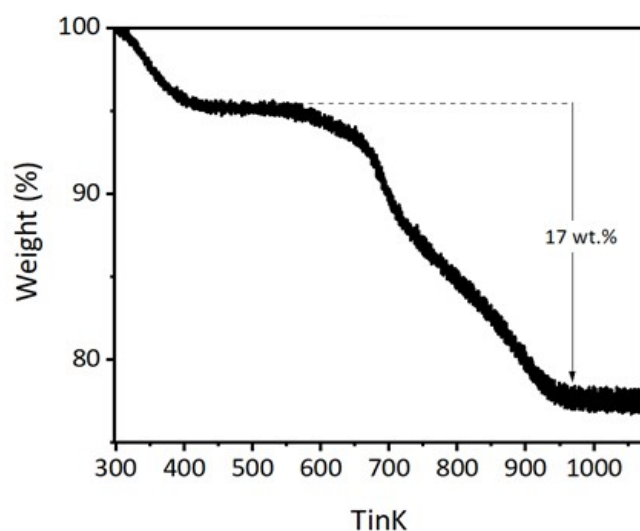


Figure S1. TGA analysis of as-prepared SAPO-34.

The X-ray powder diffraction pattern of the calcined SAPO-34 is shown in Figure S2. Small amounts of an unwanted berlinite impurity phase can be seen ($\sim 21^\circ 2\theta$) but this separate phase appears as darkened crystals of different shape under the optical microscope which were easily separated in the microspectroscopy of large SAPO-34 crystals.

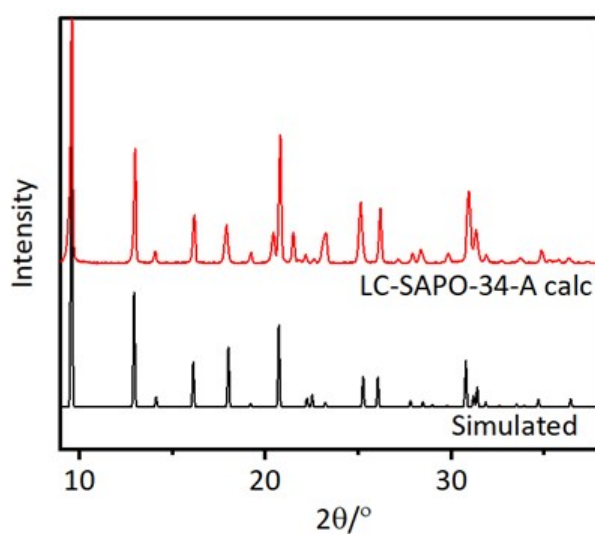


Figure S2. Powder XRD pattern of calcined SAPO-34 compared with simulated pattern.³

Cross-sectional SEM-EDX analysis of polished HSAPO-34 crystals are illustrated in Figure S3, showing a homogeneous Si distribution across crystals.

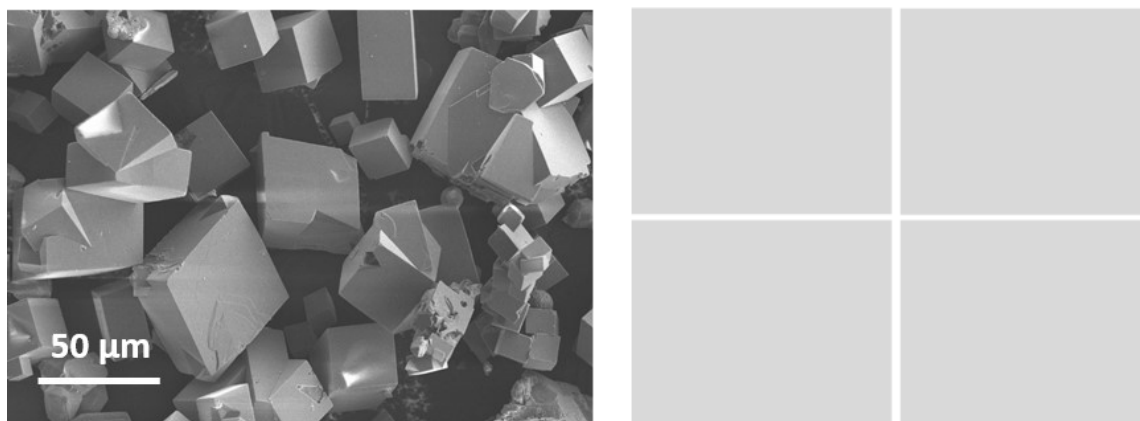


Figure S3. Left: SEM micrograph of calcined crystals of calcined SAPO-34. Right: Cross-sectional SEM-EDX analysis of a polished HSAPO-34 crystal (Si, P and Al).

The number of Brønsted acid sites in calcined HSAPO-34 was estimated from NH_3 -TPD (1.2 mmol g^{-1}), which is lower than the total silicon content from XRF (1.8 mmol g^{-1}), indicating the presence of some silicon islands which can form during synthesis at sufficiently high Si concentrations in the mother liquor. The ratios of the number of acid site to the number of Si are expected to be lower than 1 in SAPOs that contain accumulations of Si in framework positions in the lattice.⁴ The ^{29}Si NMR spectrum in Figure S4 shows the dominant signal at -94 ppm characteristic of $\text{Si}(\text{OAl})_4$ species, with some indication of components at chemical shifts < -100 due to such silicon islands.

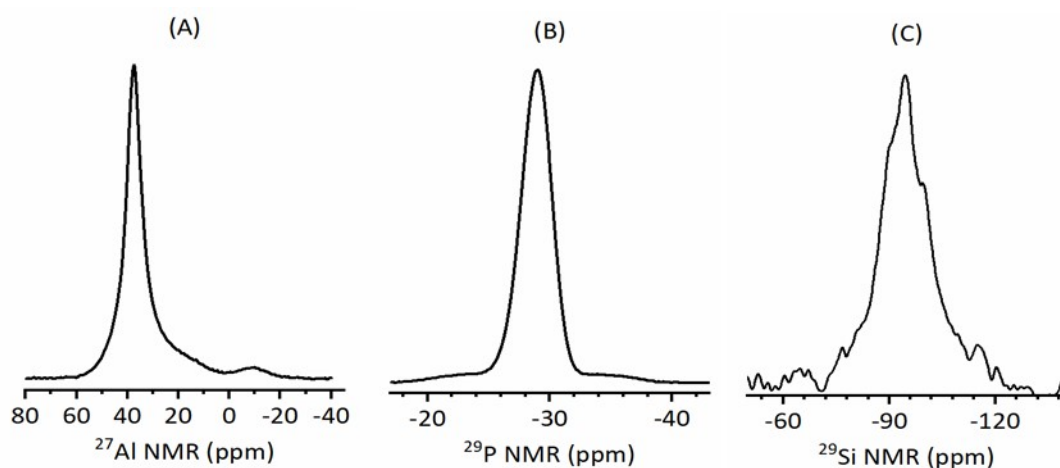


Figure S4. MAS NMR spectra of LC-SAPO-34-A calc. crystals: (A) ^{27}Al , (B) ^{31}P and (C) ^{29}Si .

2. Catalyst Evaluation.

Catalytic tests were performed in a fixed-bed stainless steel microreactor (9 mm diameter, down flow) containing quartz wool plugs and mounted inside a furnace. The calcined single crystals (0.33 g) were diluted with SiC (2.5 g, 46 grit) without prior crushing and tested for the methanol-to-olefins reaction at 723 K. During the reaction, the gas phase products were analysed by a highly customized on-line Agilent 7890B GC equipped with a RT-Q-BOND capillary column (30 m × 0.32 mm) and 2 FID and a TCD detectors for analysis of hydrocarbons C₁ to C₆, oxygenate compounds, and permanent gases respectively. Carbon mass balance was calculated using the known input flow rates of methanol and Ar/N₂ compared to the detected hydrocarbons to be 100 ± 5%. Weight hourly space velocity (WHSV) is defined as the weight of feed flowing per unit weight of the catalyst per hour. Conversion and yield are defined as the percentage of reactant converted to products.

Figure S5 shows conversion and product yield data for reaction carried out in (A) 95% CH₃OH in water and (B) 40% CH₃OH in water. As expected, these large HSAPO-34 crystals deactivate rapidly in 95% methanol, which agrees with observations made by Dai et al.⁵ After 2 min time-on-stream GC analysis was triggered and the SAPO-34 material showed a high selectivity to ethene and propene, also generating some C₄ olefins and alkanes. By the second GC analysis point at 17 min time-on-stream, rapid deactivation had occurred, and only traces of product (mostly alkane) could be detected. The catalyst lifetime of the large crystals was extended in Figure S6 (B) by using a diluted 40% methanol in water feed at reduced WHSV comparable to testing commercial microcrystalline powdered samples. Water competes with methanol for the acid sites and by doing so reduces the deactivation rate. TGA analysis of the sample recovered after the reaction revealed 3 wt.% of carbonaceous species were retained in the large SAPO-34 crystals after the MTO reaction (compared to 16 wt.% carbonaceous species in a commercial SAPO-34 powder under the same conditions), consistent with deactivation occurring in the outer rim of the crystals, as shown previously by single crystal fluorescence microspectroscopy.⁶

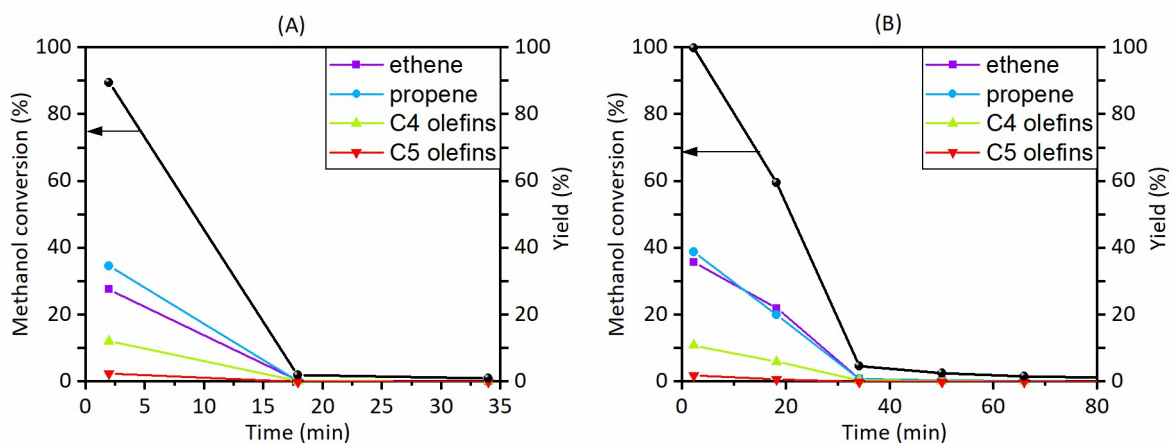


Figure S5. Effluent stream methanol conversion and olefin yields for the methanol-to-olefins reaction over calcined LC-SAPO-34-A at 723 K; the black line represents the methanol conversion. Testing conditions: (A) 95% CH₃OH in water, WHSV(CH₃OH) = 7 h⁻¹ and (B) 40% CH₃OH in water, WHSV(CH₃OH) = 2 h⁻¹

3. Supplementary Infrared and Mass Spectra.

Figure S6 gives MS data from a calibration experiment in which a 1600 s second pulse of DME was injected into the empty cell at 573 K. This shows the contribution of DME fragmentation to MS signals at 41, 31 and 27. Note in particular that the m/z = 41 contribution from fragmentation of DME is almost 3 orders of magnitude less intense than the m/z = 45 intensity, consistent with the

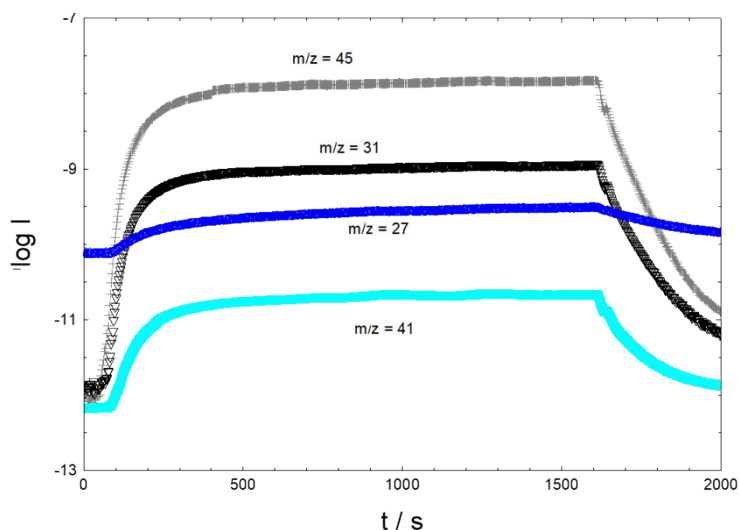


Figure S6: blank experiment with DME at 573 K in an empty cell.

fragmentation pattern reported in the NIST data base. Note also that the high baseline intensity at $m/z = 27$ is due to contribution from the adjacent $m/z = 28$ signal from the nitrogen carrier gas.

Figure S7 gives MS analysis of gases evolved when an 8 μL pulse of methanol was injected into a SAPO-34 crystal at 523 K. Only methanol and DME detected.

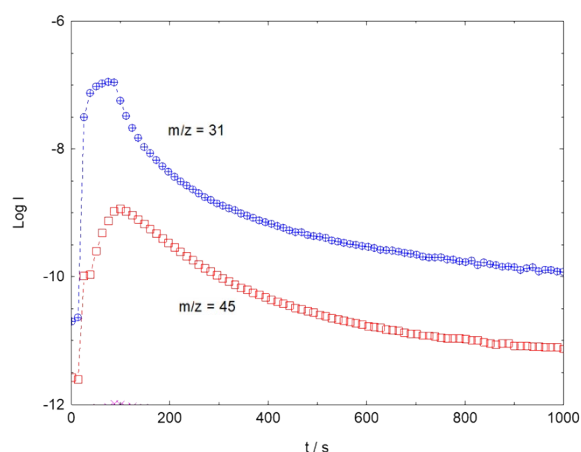


Figure S7. MS analysis of gases evolved when methanol was injected into a SAPO-34 crystal at 523 K. $m/z = 31$ measures methanol and $m/z = 45$ DME.

Figure S8 shows difference spectra recorded at 2 s intervals following exposure of a crystal of HSAPO-34 to a continuous flow of DME at 473 K. The only bands detected at this temperature are those of hydrogen bonded DME, consistent with the loss of $\nu(\text{OH})$ intensity and growth of the ABC triplet of hydrogen bonded DME. (Note that gas phase DME has not been subtracted from these difference spectra). There is no evidence of SMS formation at this temperature.

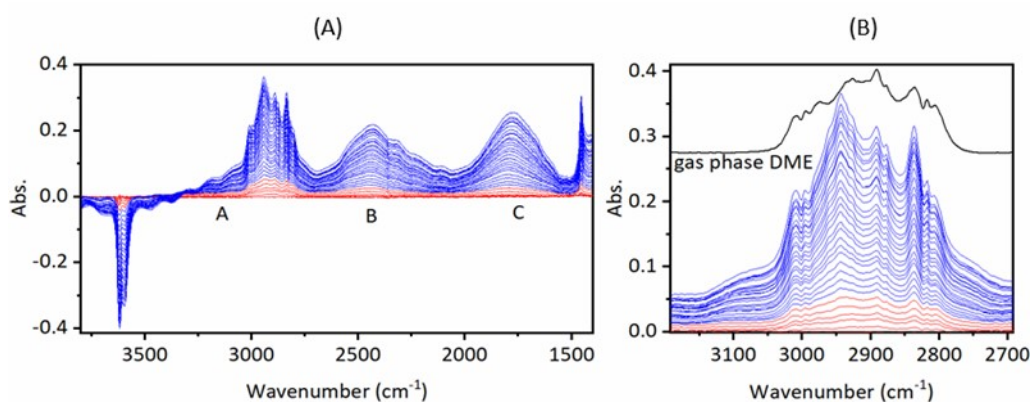


Figure S8. Difference spectra recorded at 2 s intervals during the first 64 s of continuous flow of DME into a HSAPO-34 crystal at 473 K. Colour change from red to blue 12 s after beginning DME flow.

Full range difference spectra from a similar experiment with DME at 573 K are shown in Figure S9. (The expanded $\nu(\text{CH})$ region for these spectra is Figure 6 (B) in the paper). Hydrogen-bonded DME is not observed at all when a SAPO-34 crystal is exposed to DME at 573 K.

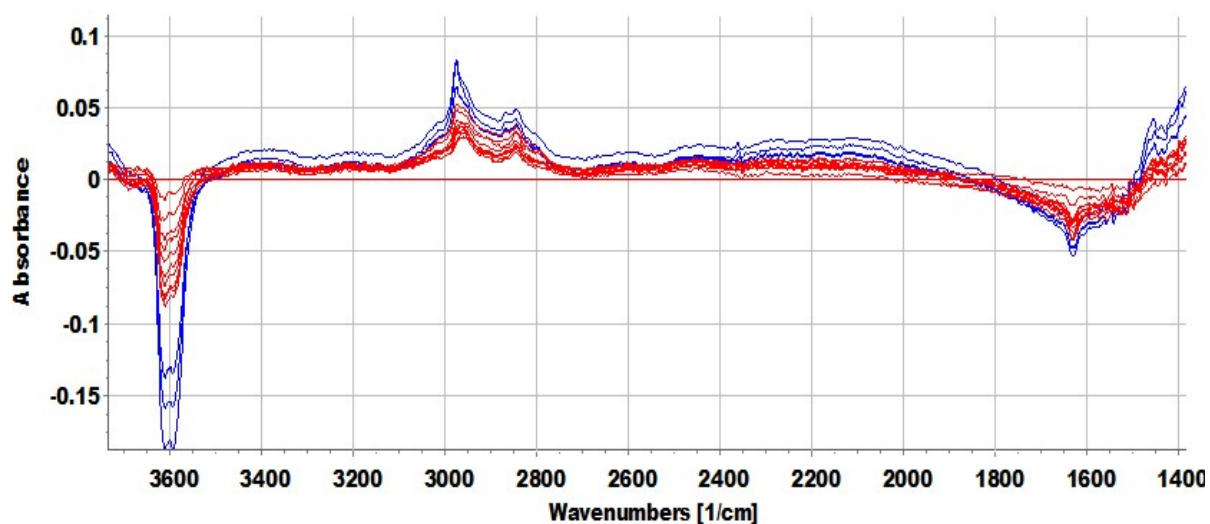


Figure S9. Difference spectra recorded during the first 80 s of continuous flow of DME into a SAPO-34 crystal at 573 K. (Gas phase DME subtracted). Red traces: first 20 s at 2 s intervals. Blue traces subsequent 60 s at 20 s intervals.

Figure S10 shows selected full-range spectra from the experiment presented in Figure 7 (methanol injection at 573 K).

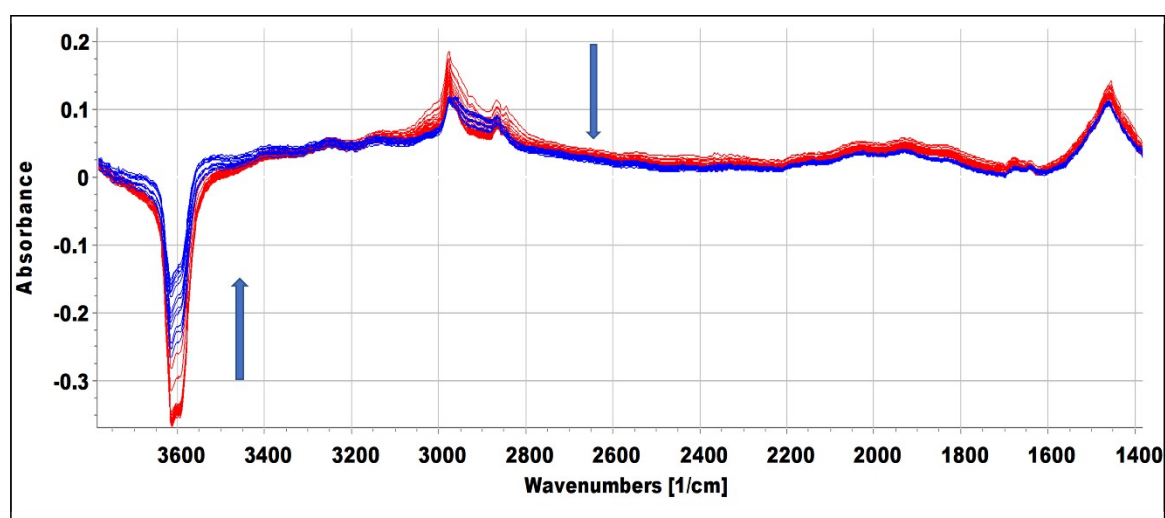


Figure S10. Difference spectra recorded following injection of an 8 μL pulse of methanol into a

SAPO-34 crystal at 573 K. Red traces: 10 s intervals from 100 s to 240 s after injection. Blue traces: 250 to 500 s after injection. Arrows indicate direction of change.

Figure S11 shows selected full-range spectra from the T-jump experiment with methanol described in Figure 9. Spectra immediately after injection of first and second methanol pulses at 523 K show SMS and hydrogen bonded DME. Immediately prior to the T jump the spectrum shows SMS and protonated DME. Immediately after the t-jump the spectrum evolves showing recovery of $\nu(\text{OH})$ intensity, loss of SMS and growth of $\nu(\text{CH})$ bands assigned to alkoxide species.

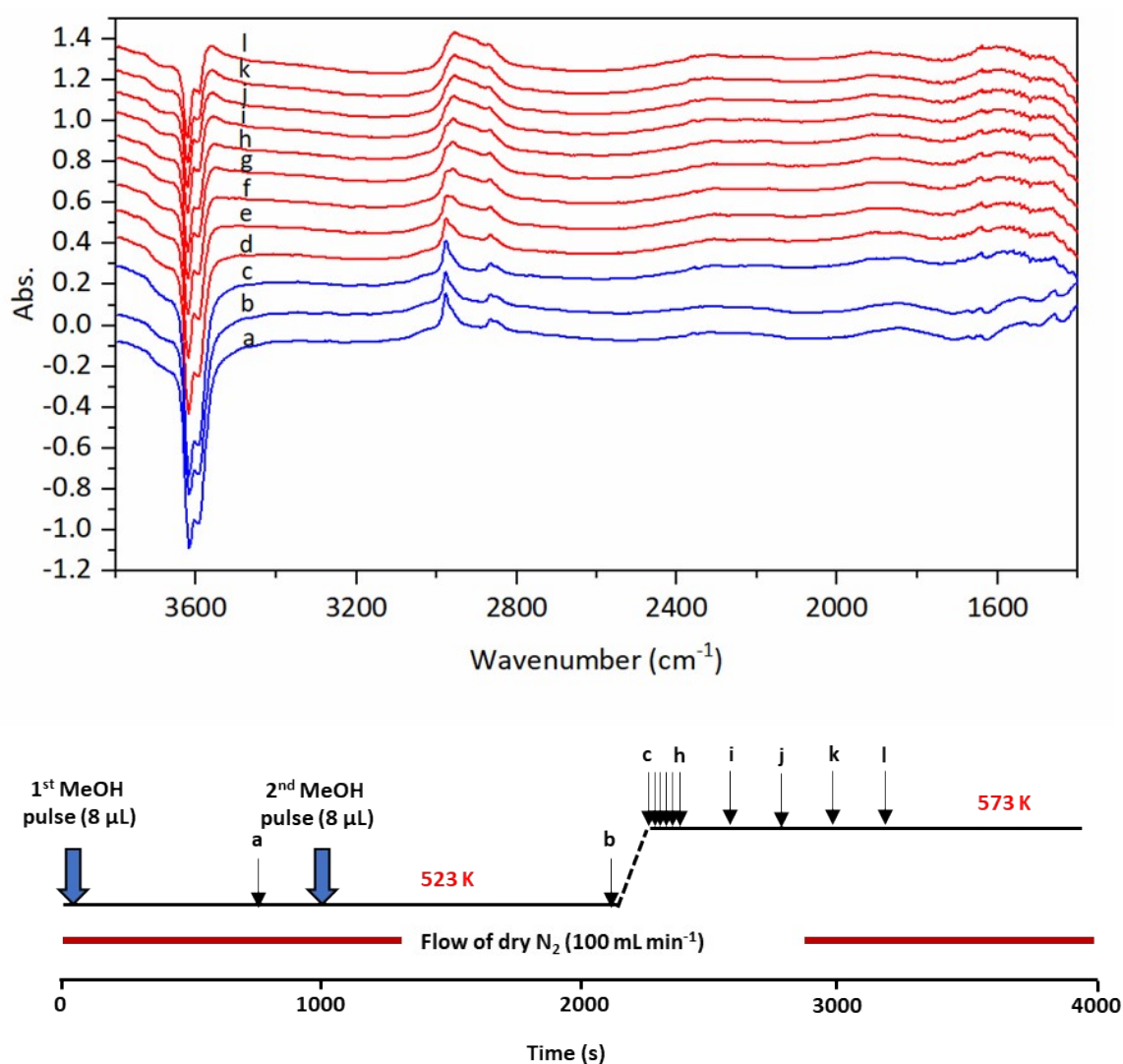


Figure S11. T-jump experiment over a SAPO-34 crystal with CH_3OH injected at 523 K. Difference FTIR spectra taken at the points marked in the schematic of this T-jump experiment.

Figure S12 shows selected full-range difference spectra from the T-jump experiment with DME presented in Figure 10 A,B,C. The spectrum during DME flow at 523 K is dominated by bands of hydrogen bonded DME. Immediately prior to the T-jump to 573 K the major species present is SMS, with only slight recovery of $\nu(\text{OH})$ intensity. Following the T-jump, SMS evolves to alkoxide species and there is a large recovery of $\nu(\text{OH})$ intensity.

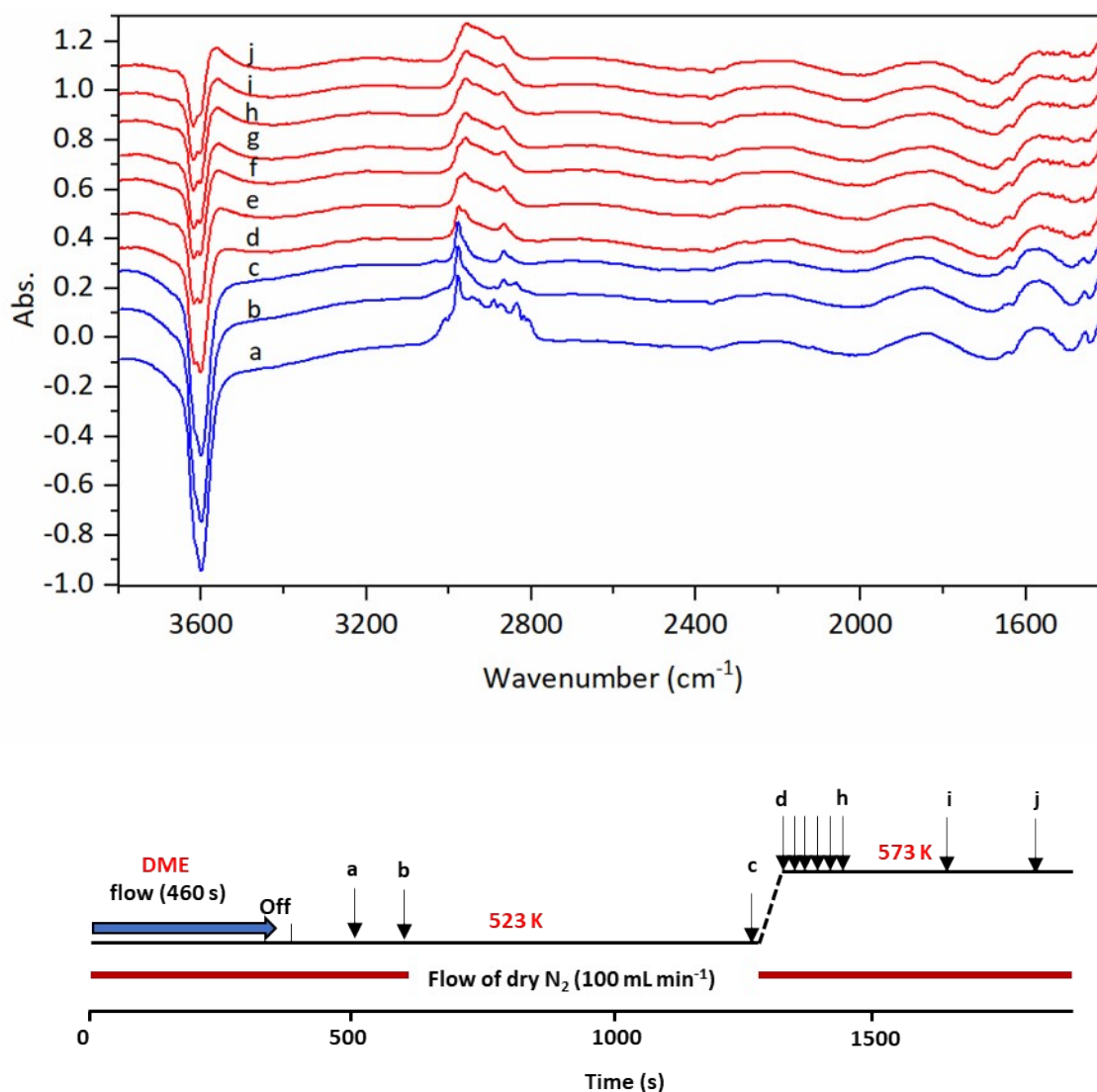


Figure S12. T-jump experiment with DME beginning at 523 K over a crystal of SAPO 34. Difference spectra taken at the points marked in the schematic of this T-jump experiment.

Figure S13 shows selected full-range spectra from the T-jump experiment with DME described in Figure 10 (D). Exposure to flowing DME at 473 K gives an intense spectrum of hydrogen bonded DME. After flushing at this temperature most of the DME is removed. The spectrum immediately prior to the first T-jump shows substantial recovery of $\nu(\text{OH})$ intensity, and weak bands of SMS and residual DME. After the first T-jump to 523 K there is little change; after the second T jump the

residual DME is completely removed and the SMS spectrum slowly evolves towards alkoxide, with a corresponding recovery of $\nu(\text{OH})$ intensity. There is little further change on subsequently ramping the temperature to 623 K.

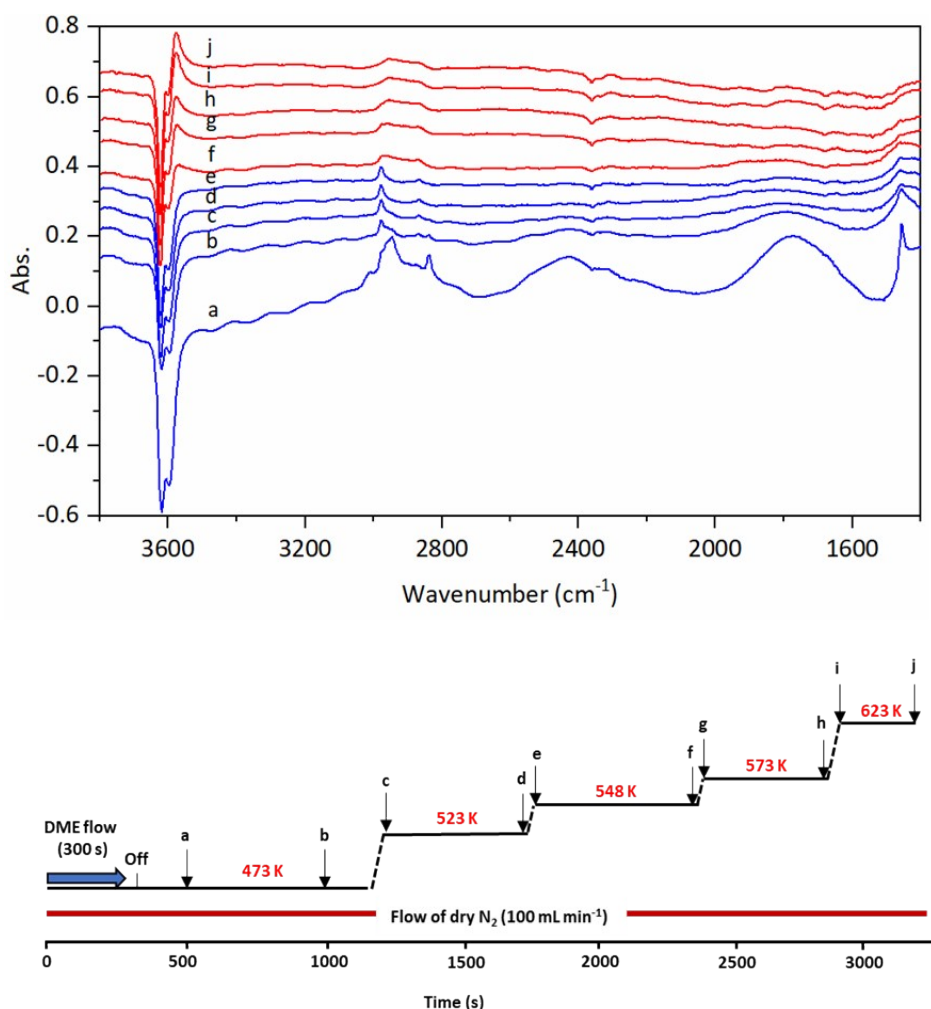


Figure S13. T-jump experiment with DME beginning at 473 K over a crystal of SAPO-34. Difference spectra taken at the points marked in the schematic of this T-jump experiment.

Figure S14 shows data from an experiment in which an 8 μL pulse of CD_3OH was injected into a SAPO-34 crystal at 623 K. The intensities at various frequencies are plotted versus time in (a) and the MS analysis of evolved gases in (b). These data show that breaking of CD bonds is accompanied by exchange of alkoxide species with OH groups of the SAPO-34. The initial loss of $\nu(\text{OH})$ intensity at 3600 cm^{-1} is due to hydrogen bonding and formation of SMS. After ~ 100 s the growth of $\nu(\text{OD})$ intensity at 2650 cm^{-1} is accompanied by growth of bands at 1464 and 2925 cm^{-1} as well as a further drop in $\nu(\text{OH})$ intensity. The MS analysis shows initial appearance of CD_3OH and DME-d_6 . The signal at $m/z = 48$ is initially due to fragmentation of the DME-d_6 , but this signal decays more slowly

than the $m/z = 50$ signal after ~ 100 s, indicating the appearance of propene- d_6 . The signal at $m/z = 47$ which grows after ~ 100 s is due to propene- d_5 .

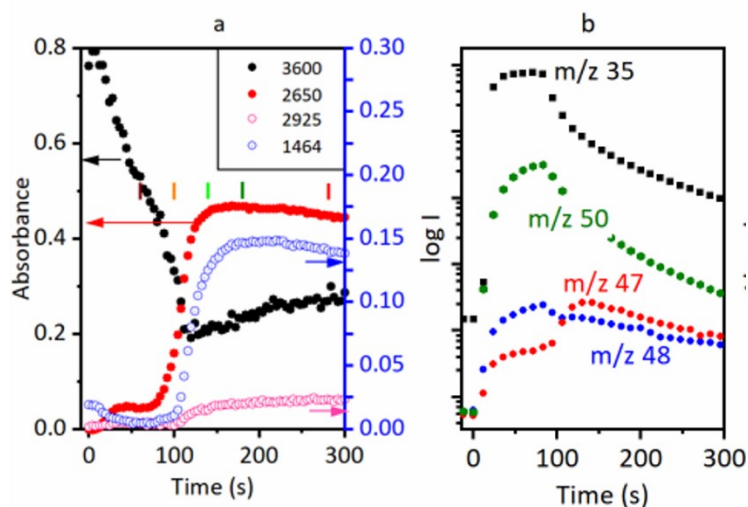


Figure S14. (a) Band intensities at the frequencies marked plotted versus time following injection of an $8 \mu\text{L}$ pulse of CD_3OH into SAPO-34 at 623 K. (b). MS analysis of evolved gases. $m/z = 35$ measures CD_3OH , $m/z = 50$ measures $\text{DME-}d_6$, $m/z = 48$ measures propene- d_6 with a contribution from fragmentation of $\text{DME-}d_6$, $m/z = 47$ measures propene- d_5 .

Figure S15 compares spectra from experiments with CH_3OH in HSAPO-34, CD_3OH in SAPO-34, CD_3OD in HSAPO-34 and CD_3OD in a 75 % exchanged DSAPO-34. The intensity of the $\nu(\text{CH})$ band at 2925 cm^{-1} depends on the amount of OH present in the experiment. The profile in the $\nu(\text{CD})$ region varies depending on the extent of H substitution into the alkoxide oligomers.

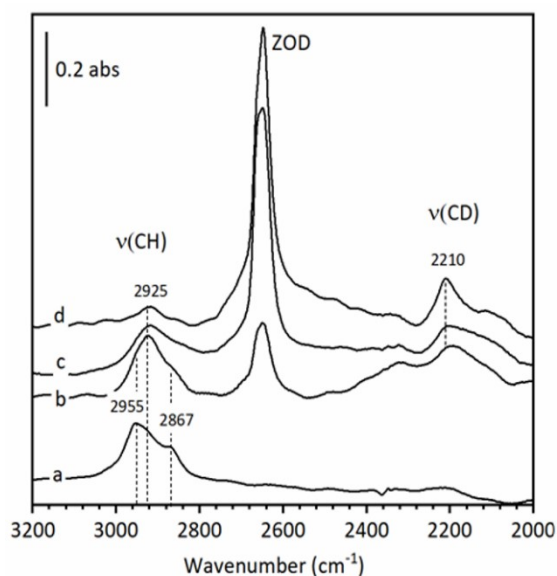


Figure S15. Difference spectra measured after injecting one 8 μ L methanol pulse into a SAPO-34 crystal at 623 K (a) CH_3OH in HSAPO-34 (b) CD_3OH in HSAPO-34. (c) CD_3OD in HSAPO-34. (d) CD_3OD in 75% exchanged DSAPO-34.

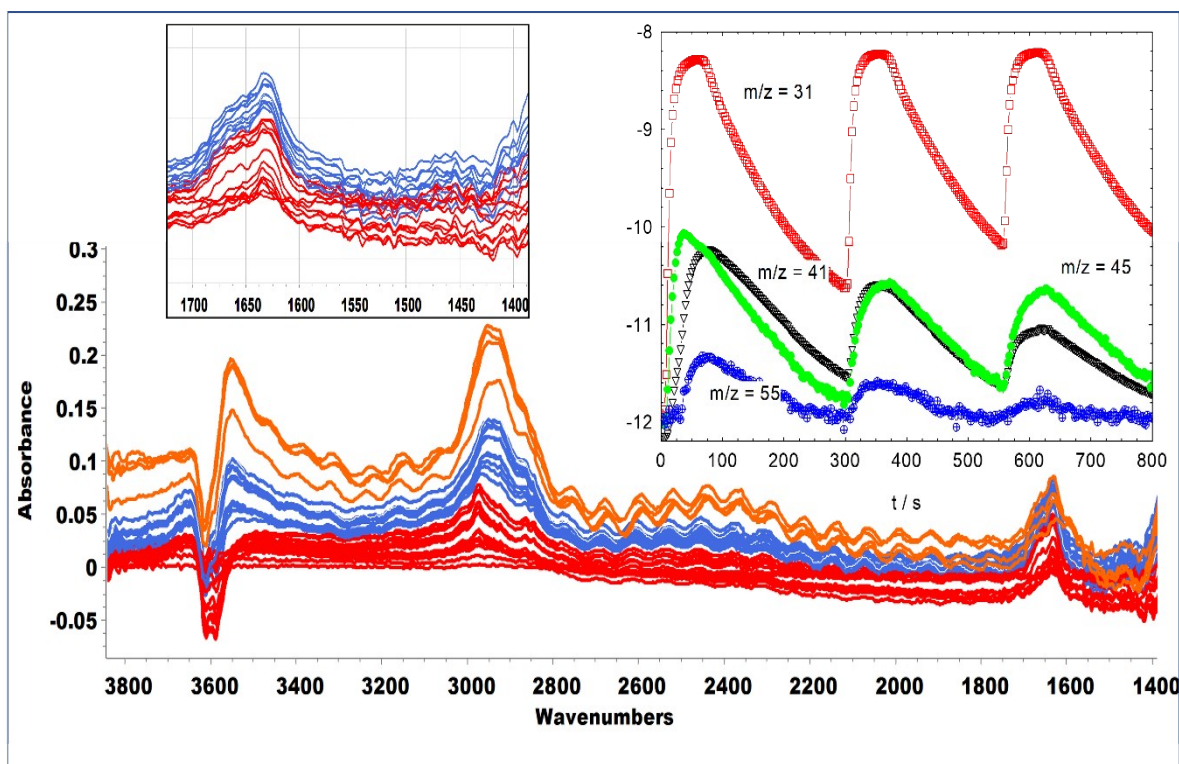


Figure S16. Difference spectra recorded during injection of three successive 8 μ L pulses of methanol at $t = 0, 300$ s and 560 s into a SAPO-34 crystal at 673 K. Red traces show spectra at 2 s intervals for 30 s following injection of the first pulse, blue traces spectra at 2 s intervals for a further 20 s, orange traces spectra measured at $t = 70, 370, 550$ and 650 s. Inset shows the MS analysis of evolved gases throughout the experiment. $m/z = 31$ measures methanol, $m/z = 45$ measures DME, $m/z = 41$ measures propene, with a contribution from fragmentation of DME, $m/z = 55$ measures butene.

DFT Calculations

To model alkoxide chains in the zeolite, linear alcohols were used. Structures were fully optimised at the B3LYP12,13/6-311G(d,p) level, followed by analytical evaluation of the harmonic vibrational frequencies (scaled by 0.9688⁸) and intensities, employing the Gaussian suite of programs.⁹ Similar methods were employed to estimate the asymmetric C=C-C stretching frequencies of cyclopentenyl cations.

To explain the $\nu(\text{CH})$ bands appearing when CD_3OH is reacted over HSAPO-34 we performed DFT calculations for different gas phase models in which H incorporation occurs at different positions in an alkane-like alkyl chain. Figure S17 shows the results obtained. (OX is an OH group). The observed $\nu(\text{CH})$ band around 2925 cm^{-1} most closely matches that calculated for H substitution into a CD_2 group of the alkoxide chain B, E or F in the Figure.

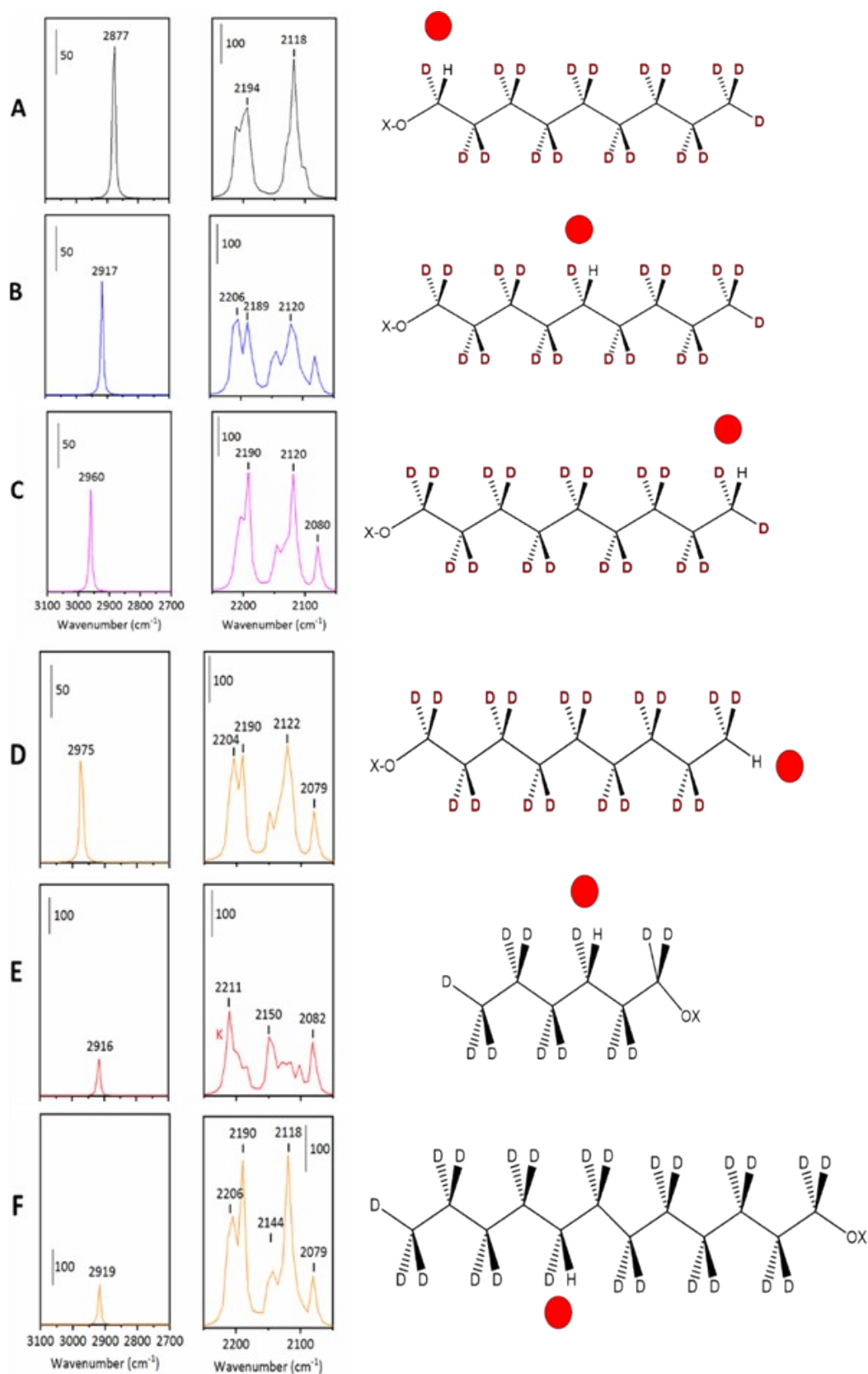


Figure S17. Calculated $\nu(\text{CH})$ and $\nu(\text{CD})$ spectra for H substituted into deuterated oligomers at different positions (marked with the red dot).

In Table S1 we compare calculated asymmetric C=C-C stretching frequencies for 1,2,3-trimethylcyclopentenyl cations containing different extents of deuterium substitution. The calculated

frequency for $C_8H_3D_{10}$ differs by only 9 cm^{-1} from that of C_8H_{13} demonstrating the relative insensitivity of the frequency to deuterium substitution. The table also shows the effect of methyl substitution at the apical position on the asymmetric stretching frequency by comparing with the 1,3-dimethylcyclopentenyl cation.

Table S1. Calculated frequencies for gas phase trimethyl cyclopentenyl cations.

$\nu_{\text{asymm}}(\text{C}=\text{C}-\text{C}^+) / \text{cm}^{-1}$

R =	CD₃	CHD₂	CH₂D	CH₃	H
1,2,3-trimethyl cyclopentenyl partially deuterated on apical carbon	1432	1439	1447	1469	
1,2,3-trimethyl cyclopentenyl(C_8H_{13})				1478 ^a	
1,3-dimethyl cyclopentenyl(C_7H_{11})				1510 ^b	1525 ^c

^a no deuterium substitution

^b experimental value in HZSM-5, see ref.²

^c experimental value in gas phase, see ref.⁷

References

1. L. Karwacki, E. Stavitski, M. H. F. Kox, J. Kornatowski and B. M. Weckhuysen, Intergrowth Structure of Zeolite Crystals as Determined by Optical and Fluorescence Microscopy of the Template-Removal Process, *Angew. Chem. Int. Ed.*, 2007, 46, 7228–7231.
2. I. B. Minova, S. K. Matam, A. Greenaway, C. R. A. Catlow, M. D. Frogley, G. Cinque, P. A. Wright and R. F. Howe, Elementary Steps in the Formation of Hydrocarbons from Surface Methoxy Groups in HZSM-5 Seen by Synchrotron Infrared Microspectroscopy, *ACS Catal.*, 2019, 9, 6564–6570.
3. Database of zeolite structures, <http://www.iza-structure.org/databases/>.
4. M. E. Potter, Down the Microporous Rabbit Hole of Silicoaluminophosphates: Recent Developments on Synthesis, Characterization, and Catalytic Applications, *ACS Catal.*, 2020, 10, 9758–9789.
5. W. Dai, G. Wu, L. Li, N. Guan and M. Hunger, Mechanisms of the Deactivation of SAPO-34 Materials with Different Crystal Sizes Applied as MTO Catalysts, *ACS Catal.*, 2013, 3, 588–596.
6. K. De Wispelaere, C. S. Wondergem, B. Ensing, K. Hemelsoet, E. J. Meijer, B. M. Weckhuysen, V. Van Speybroeck and J. Ruiz-Martínez, Insight into the Effect of Water on the Methanol-to-Olefins Conversion in H-SAPO-34 from Molecular Simulations and in Situ Microspectroscopy, *ACS Catal.*, 2016, 6, 1991–2002.
7. J. D. Mosley, J. W. Young, J. Agarwal, H. F. Schaefer, P. v R. Schleyer and M. A. Duncan, Structural isomerization of the gas-phase 2-norbornyl cation revealed with infrared spectroscopy and computational chemistry, *Angew. Chem., Int. Ed.*, 2014, 53, 5888–5891.
8. J. P. Merrick, D. Moran and L. Radom, An Evaluation of Harmonic Vibrational Frequency Scale Factors, *J. Phys. Chem. A*, 2007, 111, 11683–11700.
9. M. J. Frisch, G. W. Trucks, H. B. Schlegel, G. E. Scuseria and et al., *Gaussian 09, Revision A.02*, Wallingford CT, 2009.